On the Hydrodynamics of Finite Jets and the Geometry of Laminar Counterflow Premixed Flames

SIAVASH H. SOHRAB
Robert McCormick School of Engineering and Applied Science
Department of Mechanical Engineering
Northwestern University, Evanston, Illinois 60208
UNITED STATES OF AMERICA

http://www.mech.northwestern.edu/dept/people/faculty/sohrab.html

Abstract: - The modified form of the equation of motion at eddy-dynamic and cluster-dynamic scales is solved to describe the hydrodynamics of opposed finite jets. The results suggest that one encounters and infinite cascade of self-similar, fractal, opposed jets as the stagnation point is approached at ever-smaller spatial resolutions. Also, an analytical expression giving possible geometry of laminar premixed flames stabilized in opposed finite jets and propagating under *Huygens* principal is presented. The predicted flame geometries are found to be in agreement with the prior numerical studies as well as the observations of symmetric lean methane premixed flames at low stretch rates reported in the literature.

Key-Words: - Counterflow finite jets, stagnation flow, premixed flame geometry, *Huygens* principle.

1 Introduction

A scale-invariant statistical model of turbulence was recently employed to introduce a scale invariant model of statistical mechanics and its application to the field of thermodynamics [4]. A schematic representation of the model for the equilibrium fields of eddy-, cluster-, molecular-, and atomic-dynamics corresponding to the scales $\beta =$ e, c, m, a, and the associated non-equilibrium laminar flow fields is shown in Fig.1.

Following the classical methods [1-3], the scale-invariant forms of the conservation equations were introduced and applied to present a modified hydro-thermo-diffusive theory of laminar flames [5, 6]. Because turbulent flows are composed of ensembles of fluid elements known as turbulent eddies that are under constant chaotic motions, collisions between eddies will result in local counterflow regions. As a result, combustion studies on counterflow premixed and diffusion flames play a significant role in turbulent combustion modeling [3, 7-25]. This is because the strained induced flame stretch not only causes local flame extinction, but it also modifies the stability of the flame front surfaces [3, 7, 8, 26, 27].

In the present study, the hydrodynamics of opposed finite jets is further investigated. It will be shown that a hierarchy of counterflow fields is encountered as the stagnation point is approached at ever smaller spatial resolutions. In addition, the equation of the flame front geometry that is based on the *Huygens* principle [28, 29] is solved to determine possible premixed flame configurations in opposed finite jets. The resulting analytical solutions are compared with the experimental observation of lean methane premixed flames as well as lean and rich butane counterflow premixed flames. The results are also found to be in agreement with the earlier numerical solutions of the same problem in the literature [30-32].

2 Scale Invariant Forms of the Conservation Equations

Following the classical methods [1-3], the invariant definitions of the density ρ_β, and the velocity of *atom* $\mathbf{u}_\beta$, *element* $\mathbf{v}_\beta$, and *system* $\mathbf{w}_\beta$ at the scale β are given as [4]

$$\rho_\beta = n_\beta m_\beta = m_\beta \int f_\beta du_\beta \quad , \qquad \mathbf{u}_\beta = \mathbf{v}_{\beta-1} \qquad (1)$$

$$\mathbf{v}_\beta = \rho_\beta^{-1} m_\beta \int \mathbf{u}_\beta f_\beta d\mathbf{u}_\beta \quad , \qquad \mathbf{w}_\beta = \mathbf{v}_{\beta+1} \qquad (2)$$

Also, the invariant definitions of the peculiar and the diffusion velocities are given as [4]

$$\mathbf{V}'_\beta = \mathbf{u}_\beta - \mathbf{v}_\beta \quad , \qquad \mathbf{V}_\beta = \mathbf{v}_\beta - \mathbf{w}_\beta = \mathbf{V}'_{\beta+1} \qquad (3)$$

Next, following the classical methods [1-3], the scale-invariant forms of mass, thermal energy, and linear momentum conservation equations at scale β are given as [6]

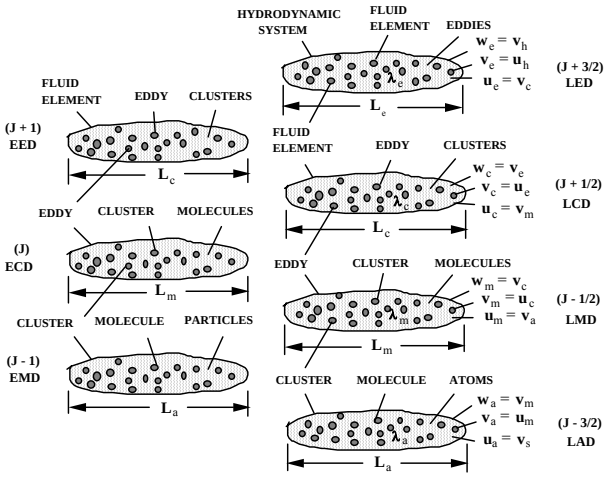

Fig.1 Hierarchy of statistical fields for equilibrium eddy-, cluster-, and molecular-dynamic scales and the associated laminar flow fields.

$$\frac{\partial \rho_\beta}{\partial t} + \nabla.\left(\rho_\beta \mathbf{v}_\beta\right) = \Omega_\beta \tag{4}$$

$$\frac{\partial \varepsilon_\beta}{\partial t} + \nabla.\left(\varepsilon_\beta \mathbf{v}_\beta\right) = 0 \tag{5}$$

$$\frac{\partial \mathbf{p}_\beta}{\partial t} + \nabla.\left(\mathbf{p}_\beta \mathbf{v}_\beta\right) = -\nabla.\mathbf{P}_\beta \tag{6}$$

involving the *volumetric density* of thermal energy $\varepsilon_\beta = \rho_\beta h_\beta$ and linear momentum $\mathbf{p}_\beta = \rho_\beta \mathbf{v}_\beta$. Also, Ω_β is the chemical reaction rate, h_β is the absolute enthalpy [5], and $\mathbf{P}_\beta$ is the partial stress tensor [1]

$$\mathbf{P}_\beta = m_\beta \int (\mathbf{u}_\beta - \mathbf{v}_\beta)(\mathbf{u}_\beta - \mathbf{v}_\beta) f_\beta du_\beta \tag{7}$$

In the derivation of (6) we have used the definition of the peculiar velocity (3) along with the identity

$$\overline{\mathbf{V}'_{\beta i}\mathbf{V}'_{\beta j}} = \overline{(\mathbf{u}_{\beta i} - \mathbf{v}_{\beta i})(\mathbf{u}_{\beta j} - \mathbf{v}_{\beta j})} = \overline{\mathbf{u}_{\beta i}\mathbf{u}_{\beta j}} - \mathbf{v}_{\beta i}\mathbf{v}_{\beta j} \tag{8}$$

The summation of (6) over all the species results in the classical form of the equation of motion [1, 3]

$$\frac{\partial \mathbf{p}_{\beta+1}}{\partial t} + \nabla.(\mathbf{p}_{\beta+1}\mathbf{v}_{\beta+1}) = -\nabla.\mathbf{P}_{\beta+1} \tag{9}$$

where $\mathbf{p}_{\beta+1} = \rho_{\beta+1}\mathbf{v}_{\beta+1}$ is the volumetric momentum density and $\mathbf{P}_{\beta+1} = \mathbf{P}$ is the total or mixture stress tensor [1, 3]

$$\mathbf{P} = \sum_\beta \mathbf{P}_\beta = \sum_\beta m_\beta \int (\mathbf{u}_\beta - \mathbf{v}_\beta)(\mathbf{u}_\beta - \mathbf{v}_\beta) f_\beta du_\beta \tag{10}$$

Following the classical methods [1], the local velocity $\mathbf{v}_\beta$ in (4)-(6) is expressed in terms of the convective $\mathbf{w}_\beta$ and the diffusive $\mathbf{V}_\beta$ velocities [5]

$$\mathbf{v}_\beta = \mathbf{w}_\beta + \mathbf{V}_{\beta g} \quad , \quad \mathbf{V}_{\beta g} = -D_\beta \nabla \ln(\rho_\beta) \tag{11a}$$

$$\mathbf{v}_\beta = \mathbf{w}_\beta + \mathbf{V}_{\beta tg} \quad , \quad \mathbf{V}_{\beta tg} = -\alpha_\beta \nabla \ln(\varepsilon_\beta) \tag{11b}$$

$$\mathbf{v}_\beta = \mathbf{w}_\beta + \mathbf{V}_{\beta hg} \quad , \quad \mathbf{V}_{\beta hg} = -\nu_\beta \nabla \ln(\mathbf{p}_\beta) \tag{11c}$$

where ($\mathbf{V}_{\beta g}$, $\mathbf{V}_{\beta tg}$, $\mathbf{V}_{\beta hg}$) are respectively the diffusive, the thermo-diffusive, the linear hydro-diffusive velocities.

Substitutions from (11a)-(11c) into (4)-(6), neglecting cross-diffusion terms and assuming constant transport coefficients with $Sc_\beta = Pr_\beta = 1$, result in [6]

$$\frac{\partial \rho_\beta}{\partial t} + \mathbf{w}_\beta.\nabla\rho_\beta - D_\beta \nabla^2 \rho_\beta = \Omega_\beta \tag{12}$$

$$\frac{\partial T_\beta}{\partial t} + \mathbf{w}_\beta.\nabla T_\beta - \alpha_\beta \nabla^2 T_\beta = -h_\beta \Omega_\beta / (\rho_\beta c_{p\beta}) \tag{13}$$

$$\frac{\partial \mathbf{v}_\beta}{\partial t} + \mathbf{w}_\beta.\nabla\mathbf{v}_\beta - \nu_\beta \nabla^2 \mathbf{v}_\beta = -\frac{\nabla p_\beta}{\rho_\beta} - \frac{\mathbf{v}_\beta \Omega_\beta}{\rho_\beta} \tag{14}$$

An important feature of the modified equation of motion (14) is that it is linear since it involves a convective velocity $\mathbf{w}_\beta$ that is different from the local fluid velocity $\mathbf{v}_\beta$. Also, the last term of the modified form of the equation of motion (14) represents a source (sink) of momentum that is induced by exothermic (endothermic) chemical reaction.

3 Symmetric Counterflow Laminar Premixed Flames

The importance of combustion in stagnation-point and counterflow burning configurations to the modeling of strained flamelets in turbulent combustion is well recognized [3, 7-25]. Therefore, the objective of the present study is to understand the structure of two identical laminar premixed flames in axi-symmetric counterflow as shown in Fig.2.

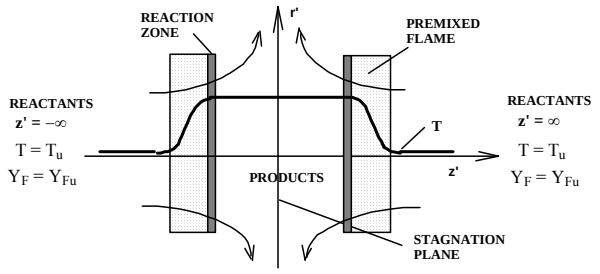

Fig.2 Schematic drawing of axi-symmetric counterflow premixed flames.

For cylindrically symmetric counter flow, the *steady* forms of (12)-(14) under the usual boundary layer assumptions and negligible pressure gradients become [6, 23]

$$w'_z \frac{dy}{dz'} = D\frac{d^2y}{dz'^2} - \Lambda y e^{\beta(\theta-1)}\delta(z'_f) \qquad (15)$$

$$w'_z \frac{d\theta}{dz'} = \alpha\frac{d^2\theta}{dz'^2} + \Lambda y e^{\beta(\theta-1)}\delta(z'_f) \qquad (16)$$

$$w'_z \frac{dv_z}{dz'} = \nu\frac{d^2v_z}{dz'^2} + v_z\Lambda y e^{\beta(\theta-1)}\delta(z'_f) \qquad (17)$$

The velocities **w** and **v** are respectively the convective and the local velocity and (z', r') are the axial and the radial coordinates. The following dimensionless parameters have been defined

$$\theta = (T - T_u)/(T_b - T_u) \quad , \quad y = Y_F/Y_{Fu}, \qquad (18)$$

$$\rho = \rho_{Fu} = \rho Y_{Fu} \quad , \quad \Lambda \equiv (\nu_F W_F B/\rho)\, e^{-\beta/\chi} \qquad (19)$$

The adiabatic flame temperature T_b, the *Zeldovich* number β, and the coefficient of thermal expansion χ are

$$T_b = T_u + QY_{Fu}/\nu_F W_F c_p \qquad (20)$$

$$\beta = E(T_b - T_u)/RT_b^2 \quad , \quad \chi = (T_b - T_u)/T_b \qquad (21)$$

and one assumes that $\beta >> 1$. Also, unity *Prandtl* Pr = ν/α, *Schmidt* Sc = ν/D, and *Lewis* Le = α/D numbers are assumed, such that θ, y, and ν fields will be similar under identical boundary conditions.

The solutions of the system (15)-(17) outside of the thin reaction zone where $\Lambda = 0$ provide the hydro-thermo-diffusive structure of the counterflow premixed flame presented earlier [25]

$$\theta = 1 - y = \frac{1}{2}\mathrm{erfc}(\zeta_c - \zeta_f) \qquad (22)$$

$$v_{zc} = -v_f - \frac{v_b}{2}\mathrm{erfc}(\zeta_c - \zeta_f) \qquad (23)$$

In the following, the hydrodynamics of such counterflow finite jets and the geometry of premixed flames stabilized in such flow fields will be investigated.

4 Hydrodynamics of Cylindrically Symmetric Counterflow Finite Jets

The solution of the modified equation of motion for the classical problems of laminar axi-symmetric stagnation-point flow and counterflow jets were discussed in a previous study [24]. It was shown that the flow field outside of the thin boundary layer must be determined at the scale of LED with the relevant "atomic", element, and system velocities ($\mathbf{u}_e$, $\mathbf{v}_e$, $\mathbf{w}_e$) and the associated length scales ($l_e = 10^{-5}$, $\lambda_e = 10^{-3}$, $L_e = 10^{-1}$) m. The convective velocity for this outer flow is known and given by [2]

$$w'_{re} = \Gamma_e r' \quad , \quad w'_{ze} = -2\Gamma_e z' \qquad (24)$$

where the velocity gradient is the ratio of the jet velocity at the nozzles w'_{zo} and the thickness of the hydrodynamic "boundary layer" δ_f

$$\Gamma_e = w'_{zeo}/\delta_f \qquad (25)$$

to be further described in the following. The subscript (e) refers to the laminar eddy-dynamic (LED) scale β = e and the relevant kinematic viscosity for this scale is $\nu_e = l_e u_e/3 = \lambda_c v_c/3$ [5]. One also introduces the dimensionless velocities

$$(\mathbf{v_{re}}, \mathbf{v_{ze}}, \mathbf{w}_{ze}) = (\mathbf{v'_{re}}, \mathbf{v'_{ze}}, \mathbf{w}'_{ze})/\sqrt{\nu_e\Gamma_e} \qquad (26)$$

and coordinates

$$\xi_e = r'/\sqrt{\nu_e/\Gamma_e} \quad , \quad \zeta_e = z'/\sqrt{\nu_e/\Gamma_e} \qquad (27)$$

The solution of (17) in the absence of reaction and with the convective velocity (24) under the appropriate boundary conditions was shown to result in the stream function [24]

$$\Psi_e = -\xi_e^2\ \mathrm{erf}(\zeta_e) \qquad (28)$$

and hence the velocities

$$v_{ze} = -2\mathrm{erf}(\zeta_e) \qquad (29)$$

$$v_{re} = \frac{2}{\sqrt{\pi}} \xi_e \exp(-\zeta_e^2) \qquad (30)$$

The axial and radial velocity profiles calculated from (29)-(30) are shown in Fig.3 and are in qualitative agreement with the experimental observations in Fig.8 of *Tsuji* and *Yamaoka* [16].

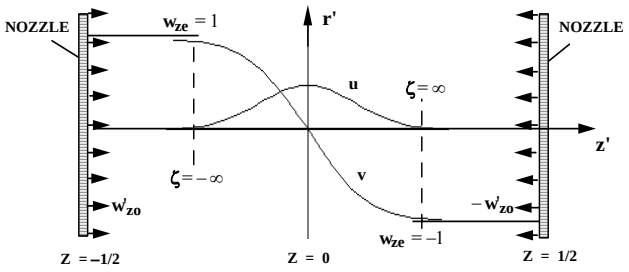

Fig.3 Calculated velocity profiles for axi-symmetric finite-jet counterflow ($u = v_{re}$, $v = v_{ze}$) from (29)-(30).

Some of the streamlines calculated from (28) are shown in Fig.4.

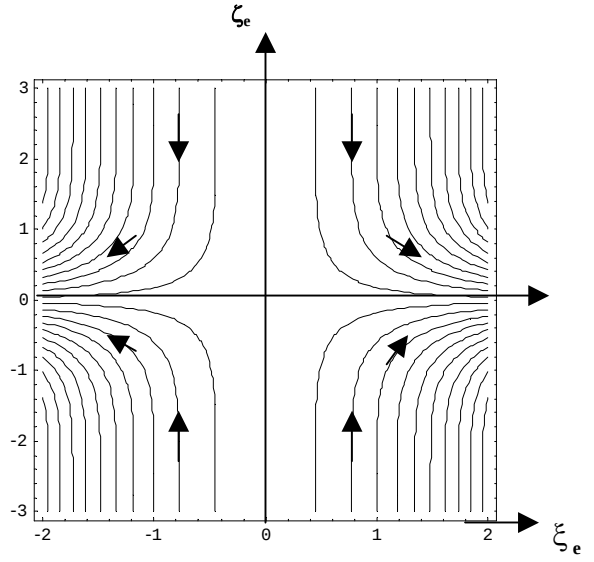

Fig.4 Calculated streamlines from (28) for axi-symmetric opposed finite jets.

According to (28), the jets do not diverge until they reach the position of the hydrodynamic "boundary layer" (Fig.4) that corresponds to the inner scale $\zeta_c \to \infty$ (Fig.3). The thickness of the boundary layer at LED scale is obtained from the solution (28) as the location $\zeta_e^* \simeq 2.4$ where the streamlines no longer change with ζ to an accuracy of 0.9995 [24]

$$\delta_f = L_e \simeq 2.4\sqrt{\frac{\nu_e}{\Gamma_e}} \qquad (31)$$

in exact agreement with the classical result [2].

The choice of 2.4 in (31) was to show the close agreement with the classical exact numerical solution of the *Navier-Stokes* equation [2]. However, to facilitate the scaling problem discussed below the choice of $\zeta_e^* \approx 2.0$ will be made that defines the edge of boundary layer to the accuracy of 0.995. At $\zeta_e^* \approx 2.0$ the axial velocity at the edge of the boundary layer $v_{ze}'^*$ from (29) will be

$$v_{ze}'^* = -2\sqrt{\Gamma_e \nu_e} \qquad (32)$$

With the definition of the stretch rate as

$$\Gamma_e = \frac{w_o'}{L_e} = \frac{w_o'}{\delta_f} \qquad (33)$$

one obtains from (32)

$$v_{ze}'^* / w_o' \simeq 1 = 2\sqrt{\frac{\nu_e}{w_o' L_e}} = \frac{2}{\sqrt{Re_e}} \qquad (34)$$

resulting in the *Reynolds* number

$$Re_e = \frac{w_o' L_e}{\nu_e} \simeq 4 \qquad (35)$$

Also, with $\zeta_e^* \approx 2$ the edge of the boundary layer (31) will be modified as

$$L_e = \delta_f \approx 2\sqrt{\frac{\nu_e L_e}{w_o'}} = 2\frac{L_e}{\sqrt{Re_e}} \qquad (36)$$

that is in accordance with (35).

As the streamlines in Fig.4 show, the important hydrodynamic length is the thickness of the boundary layer δ_f rather than the separation distance between the nozzles L, as long as $L > \delta_f$. This is to be expected since beyond this boundary the streamlines are parallel and no longer change (Figs.3, 4) and the position of burner nozzles has no impact on the hydrodynamic problem. The Reynolds number may be expressed as the ratio of outer to inner length scales

$$\mathrm{Re}_e = \frac{L_e w'_o}{\nu_e} = \frac{L_e}{(\nu_e / w'_o)} = \frac{L_e}{\delta_e} = \frac{\delta_f}{\delta_e} \simeq 4 \qquad (37)$$

where the inner length scale is defined as

$$\delta_e = \nu_e / w'_o \qquad (38)$$

and represents the characteristic length for diffusion of momentum. The approximate scaling factor of 4 between the outer and the inner hydrodynamic lengths (36) was also arrived at in the earlier investigations [6, 24, 25].

In the neighborhood of the stagnation point, $\zeta_e \ll 1$ and $\xi_e \ll 1$ the solutions (29)-(30) lead to

$$v_{ze} = -\frac{4}{\sqrt{\pi}}\zeta_e \quad , \quad v_{re} = \frac{2}{\sqrt{\pi}}\xi_e \qquad (39)$$

that in view of (26) and (27) could be expressed as

$$v'_{ze} = w'_{zc} = -\frac{4}{\sqrt{\pi}}\Gamma_e z' = -2\Gamma_c z' \qquad (40)$$

$$v'_{re} = w'_{rc} = \frac{2\Gamma_e}{\sqrt{\pi}} r' = \Gamma_c r' \qquad (41)$$

when one has introduced the following new definition

$$\Gamma_c = \frac{2}{\sqrt{\pi}}\Gamma_e \qquad (42)$$

for the stretch rate at LCD scale.

The local velocities (v'_{re}, v'_{ze}) at LED scale in (40)-(41) also represent the convective velocities (w'_{rc}, w'_{zc}) for the next lower scale of LCD

$$w'_{rc} = \Gamma_c r' \quad , \quad w'_{zc} = -2\Gamma_c z' \qquad (43)$$

that have the same form as the velocity of the outer flow (24). The flow within the thin viscous boundary layer at LCD scale will have the length scales $(l_c = 10^{-7},\ \lambda_c = 10^{-5},\ L_c = 10^{-3})$ m. One can therefore introduce the new coordinates

$$\xi_c = r' / \sqrt{\nu_c / \Gamma_c} \quad , \quad \zeta_c = z' / \sqrt{\nu_c / \Gamma_c} \qquad (44)$$

with the new stretch rate Γ_c defined in (42). The solution of the equation of motion (17) at this smaller scale of LCD with the convective field (43) and under the same boundary conditions as those of the outer flow will be identical to (28)-(30).

The above result is also supported by the fact that near the stagnation point of counterflow jets, because of the viscous effects, a small region of secondary flow recirculation will be established. Such a flow field is formed by two semi-spherical "Hill vortices" obtained from the exact solution of the dimensionless modified *Helmholtz* vorticity equation [33, 34]

$$\mathbf{w}_r \frac{\partial \omega_\theta}{\partial \xi} + \mathbf{w}_z \frac{\partial \omega_\theta}{\partial \zeta} = -\frac{\mathbf{w}_r \omega_\theta}{\xi} + \left[\frac{\partial^2 \omega_\theta}{\partial \xi^2} + \frac{1}{\xi}\frac{\partial \omega_\theta}{\partial \xi} - \frac{\omega_\theta}{\xi^2} + \frac{\partial^2 \omega_\theta}{\partial \zeta^2} \right] \qquad (45)$$

given by the stream function

$$\Psi = \xi^2 \zeta\ (1 - \xi^2 - \zeta^2) \qquad (46)$$

Some of the streamlines from (46) along with the streamlines for counterflow jets from (28) are shown in Fig.5 where the diameter of the spherical flow region is exaggerated for clarity.

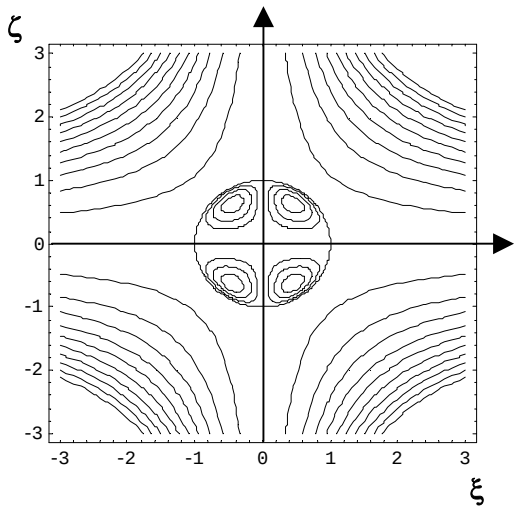

Fig.5 Spherical flow recirculation zone near the stagnation point of viscous counter flow [34].

The actual radius of this zone $r^* = \sqrt{\nu_e / \Gamma_e}$ will depend on the fluid kinematic viscosity and the stretch rate [34].

Examination of Fig.5 shows that the streamlines near the origin are identical to those of the outer cylindrically symmetric counter flow jets in accordance with the suggestion made above. Therefore, in view of the linearity of (45), one obtains a product solution for two concentric spherical flows with radii (R_1, R_2) given by [34]

$$\Psi = \Psi_1 \Psi_2 = \xi^4 \zeta^2 (R_1 - \xi^2 - \zeta^2)(R_2 - \xi^2 - \zeta^2) \qquad (47)$$

The direction of rotation of the adjacent generations of such concentric spherical flows will alternate [34]. Such a hierarchy of concentric spherical flows also suggests that one should expect a cascade of self-similar, fractal, counterflows at scales LCD, LMD, LAD, …(Figs.1, 5) as the stagnation point is approached at ever-smaller spatial resolutions.

The central significance of the above results is in connection to the important problem of turbulent dissipation addressed by *Heisenberg* [35]. Since *Richardson's* well-known rhyme concerning big and little eddies, turbulent fluctuations are generally assumed to carry motions from the large integral scales down the *Kolmogorov* dissipative scale. However, no clear mechanism for transfer of vorticity across such cascades of scales has been identified. Because turbulent flows are composed of eddies whose collisions generate local counterflows, the formation of hierarchy of concentric spherical flows at the stagnation regions of such counterflows, Fig.5, could be considered as a mechanism for transport of vorticity to the dissipative scales.

The above results are also harmonious with the scale-invariant logarithmic definition of coordinates that was recently introduced [36] where the coordinate at scale β is related to that at the lower adjacent scale β −1 as schematically shown below

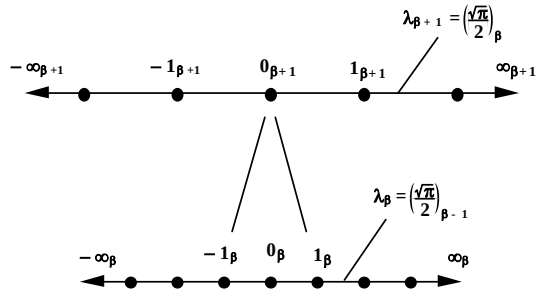

Fig.6 Hierarchy of normalized coordinates for cascades of embedded statistical fields [35].

In view of Fig.6, the range $(-1_{\beta},1_{\beta})$ of the outer coordinate x_{β} will correspond to the range $(-\infty_{\beta-1},\infty_{\beta-1})$ of the inner coordinate $x_{\beta-1}$ while the zero of the higher scale $(-0_{\beta},+0_{\beta})$ decompactifies to the unity $(-1_{\beta-1},1_{\beta-1})$ of the lower scale as shown in Fig.6. The analogy between the hierarchy of counterflow finite jets shown in Fig.3 and the hierarchy of embedded finite interval $(-1_{\beta},1_{\beta})$ on a line shown in Fig.6 thus provides a *physical basis* for the invariant model of analysis described earlier [36]. The analogy is further enhanced by the fact that the solution of the velocity field (29) involves *Gauss's* error function that also formed the basis for the "measure" employed for the normalization of coordinates [36].

6. Geometry of Counterflow Finite-Jet Premixed Flames

The equation that governs the dynamics of the premixed flame geometry has been investigated on the basis of *Huygens* principle [28, 29]. In this section, possible flame configurations for premixed flames stabilized in counterflow finite jets will be examined. Some typical direct photographs of flame taken by the author are shown in Fig.7a-7c.

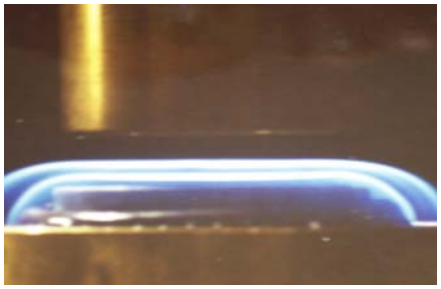

(a)

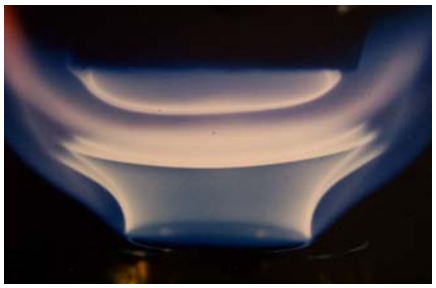

(b)

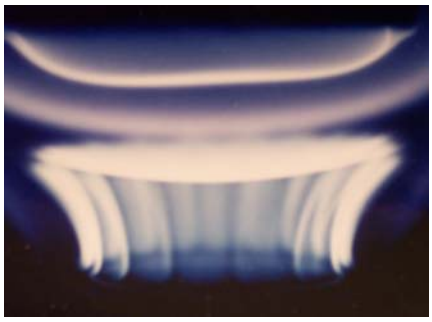

(c)

Fig.7 Premixed flame geometries in opposed finite jets (a) symmetric lean premixed flames (b) lean and rich butane-air premixed flames separated by a diffusion flame (c) lean and rich butane-air premixed flames with the latter flame showing cellular instability.

The flame geometry will depend on the relative magnitude of the jet axial velocity at nozzle w'_{zo} versus the laminar flame propagation velocity v'_{f}, and

the rate of stretch Γ_e(23) that also depends on the axial velocity at the nozzles (Figs.2, 4).

The geometry of the premixed flame stabilized in the vicinity of the stagnation point can be obtained from the equation [28, 29]

$$\frac{\partial G}{\partial t} + \mathbf{w}.\nabla G = v_f |\nabla G| \tag{48}$$

The flame surface is expressed as

$$G = \xi - g(\zeta, t) \tag{49}$$

that involves the dimensionless quantities

$$G = G'\sqrt{\Gamma_e/\alpha} \quad , \quad g = g'\sqrt{\Gamma_e/\alpha} \tag{50}$$

and the laminar flame propagation velocity

$$v_f = v_f'/\sqrt{\Gamma_e \alpha} \tag{51}$$

The unit vector normal to the flame surface and the convective velocity field are given by

$$\mathbf{n} = -\frac{\nabla G}{|\nabla G|} = -\frac{\hat{\xi} - g_\zeta \hat{\zeta}}{\sqrt{1+g_\zeta^2}} \tag{52}$$

$$\mathbf{w} = \xi\hat{\xi} - 2\zeta\hat{\zeta} \tag{53}$$

For the steady flame configuration, by substitution from (49)-(53) one obtains from (48)

$$\left(\frac{\partial g}{\partial \zeta}\right)^2 (4\zeta^2 - v_f^2) + 4\xi\zeta\left(\frac{\partial g}{\partial \zeta}\right) + \xi^2 - v_f^2 = 0 \tag{54}$$

The above nonlinear equation has a closed form analytical solution

$$g = -\frac{\xi}{4}\ln(4\zeta^2 - B^2) \pm \left\{ \frac{B}{\sqrt{\Delta}} \text{Arc}\tan\left(\frac{4\zeta}{\sqrt{\Delta}}\right) - \frac{\xi}{4}\ln\left[\frac{\sqrt{\xi^2 R'} + \xi^2 t' + B}{\sqrt{\xi^2 R''} + \xi^2 t'' - B}\right] \right\} \tag{55}$$

Substituting from (55) in (49) gives the flame surface geometry as

$$G(\xi,\zeta) = \xi - \frac{\xi}{4}\ln(4\zeta^2 - B^2) + \frac{B}{\sqrt{\Delta}}\text{Arc}\tan(\frac{4\zeta}{\sqrt{\Delta}}) - \frac{\xi}{4}\ln\left[\frac{\sqrt{\xi^2 R'} + \xi^2 t' + B}{\sqrt{\xi^2 R''} + \xi^2 t'' - B}\right] \tag{56}$$

The following definitions have been introduced

$$\Delta = 4(\xi^2 - B^2) \tag{57}$$

$$R' = 1 + 2Bt' + \xi^2 t'^2 \tag{58}$$

$$R'' = 1 - 2Bt'' + \xi^2 t''^2 \tag{59}$$

$$t' = \frac{1}{2\zeta - B} \quad , \quad t'' = \frac{1}{2\zeta + B} \tag{60}$$

along with the important parameter representing the dimensionless flame propagation velocity

$$B = \frac{v_f'}{\sqrt{\Gamma_e \alpha}} \tag{61}$$

where α is the thermal diffusivity that is assumed to be equal to the kinematic viscosity under the unity *Prandtl* number $\alpha = \nu$ assumption being adopted.

The calculated flame geometry from (56) are shown in Fig.8 for a typical dimensionless flame propagation speed B = 0.02.

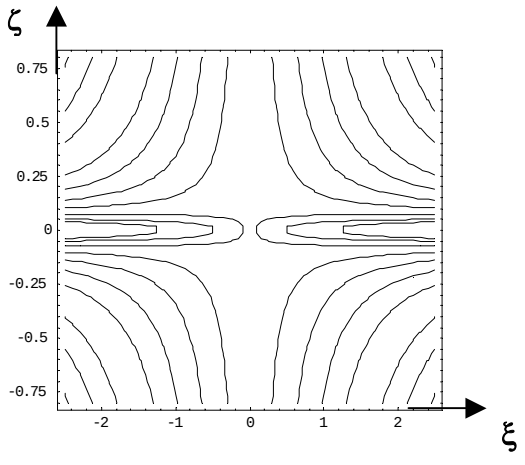

Fig.8 Possible geometry of premixed flame surfaces in symmetric opposed finite jets.

The sharp edges at the crossing of the conical funnel-shaped flame and the planar flame in Fig.7b are optical path effects of the flame photograph. The particular flame shape involving a hole when the upper and lower planar flame surfaces join near the jet axis of symmetry leaving a small hole in the

vicinity of the stagnation point was first reported in a direct photograph by *Ishizuka* and *Law* [19]. For the case of rich butane-air flames, the outer conical flame can become thermo-diffusively unstable and assume the shape of a polyhedral flame as shown in Fig.7c.

For the solution (56) to be physically meaningful, involve real rather than imaginary numbers, one must impose the requirements

$$\xi^2 > B^2 \quad , \quad 4\zeta^2 > B^2 \qquad (62)$$

Therefore, there will be a forbidden zone in the vicinity of the stagnation point within which the flow velocity is everywhere smaller than the flame speed and hence cannot support a stable and stationary flame front in accordance with the previous studies [30-33]. The size of the hole will be a function of the flame propagation velocity and the stretch rate (v_f', Γ_e).

8 Concluding Remarks

Scale-invariant forms of the conservation equations were solved for the problem of counterflow finite jets. It was shown that the solution suggest the occurrence of a hierarchy of counterflows at ever-smaller scales as one approaches the stagnation point. Also, an analytical solution for the geometry of counterflow premixed flames stabilized in finite jets was presented. In view of the predominance of locally strained counterflows in turbulent fields, the understanding of the various flame configurations in such flows will play a central role in the future comprehensive models of turbulent combustion.

Acknowledgements:
This research was in part supported by NASA micro-gravity combustion science program under grant NAG3-1863.

References:

[1] de Groot, R. S., and Mazur, P., *Nonequilibrium Thermodynamics*, North-Holland, 1962.
[2] Schlichting, H., *Boundary-Layer Theory*, McGraw Hill, New York, 1968.
[3] Williams, F. A., *Combustion Theory*, 2nd Ed., Addison-Wesley, New York, 1985.
[4] Sohrab, S. H., *Rev. Gén. Therm.***38**, 845 (1999).
[5] Sohrab, S. H., *WSEAS Transactions on Mathematics*, Issue 4, Vol.3, 755 (2004).
[6] Sohrab, S. H., *WSEAS Transactions on Fluid Mechanics*, Issue 5, Vol.1, 337 (2006).
[7] Liñán, A., The asymptotic structure of counterflow diffusion flames for large activation energies. *Acta Astronautica* **1**, 1007 (1974).
[8] Peters, N., *Proc. Combust. Inst.* 20, p. 1231 (1986).
[9] Warnatz, J., Maas, U., and Dibble, R. W., *Combustion,* Springer, New York, 1996.
[10] Buckmaster, J. D., and Ludford, G. S. S., *Theory of Laminar Flames*, Cambridge University Press, Cambridge, 1982.
[11] Saitoh, T., and Otsuka, Y., *Combust. Sci. Technol.* **12**, 135 (1976).
[12] Daneshyar, H., Mendes-Lopes, J. M. C., and Ludford, G. S. S., *Proc. Combust. Inst.* 19, p. 413 (1982).
[13] Seshadri, K., *Int. J. Engin. Sci.* **21**, 103 (1983).
[14] Stahl, G., and Warnatz, J., *Combust. Flame* **85**, 285 (1991).
[15] Sohrab, S. H., Ye, Z. Y., Law, C. K., *Combust. Sci. Technol.* **45**, 27 (1986).
[16] Yamaoka, I., and Tsuji, H., *Proc. Combust. Inst.* 17, 843 (1978).
[17] Tsuji, H., and Yamaoka, I., *Proc. Combust. Inst.* 19, 1533 (1982).
[18] Tsuji, H., and Yamaoka, I., *Proc. Combust. Inst.* 20, 1883 (1984).
[19] Ishizuka, S., and Law, C. K., *Proc. Combust. Inst.*19, 327 (1982).
[20] Sato, J., *Proc. Combust. Inst.* 19, 1541 (1982).
[21] Wu, C. K., and Law, C. K., *Proc. Combust. Inst.* 20, 1941 (1984).
[22] Sohrab, S. H., Ye, Z. Y., and Law, C. K., *Proc. Combust. Inst.*20, 1957 (1984).
[23] Kurz, O., and Sohrab, S. H., *First Joint Western-Central-Eastern States Section Meeting*, The Combustion Institute, March 14-17, 1999, George Washington University, Washington DC.
[24] Sohrab, S. H., *IASME Transactions*. Issue **7**, Vol.2, 1097 (2005).
[25] Sohrab, S. H., *WSEAS Transactions on Fluid Mechanics*, Issue **1**, Vol.1, 31 (2006).
[26] Sivashinsky, G. I, *Annual Review of Fluid Mechanic* **15**, 179 (1983).
[27] Clavin, P., *Prog. Energy Combust. Sci.* **11**, 1, (1985).
[28] Williams, F. A., in, *The Mathematics of Combustion.* J. D. Buckmaster (Ed.), 1985, SIAM Philadelphia.
[29] Kerstein, A. R., Ashurst, W. T., and Williams, F. A., *Phys. Rev.* A **37**, 2728 (1988).
[30] Sheu, W. J. and Sivashinsky, G, I., *Combust. Flame* **84**, 221 (1991).
[31] Brewster, M. E., *Combust. Flame* **91**, 99 (1992).
[32] Sung, C. J., Trujillo, J. Y. D., and Law, C. K *Combust. Flame* **103**, 247 (1995).
[33] Sohrab, S. H., *5Th International Microgravity Combustion Workshop* NASA, May 18-20, 1999, Cleveland, Ohio.
[34] Sohrab, S. H., *IASME Transactions,* Issue **4**, Vol.1, 634 (2004).
[35] Heisenberg, W., *Proc. R. Soc. London, Ser. A* **195**, 402 (1948).
[36] Sohrab, S. H., *11th WSEAS International Conference on Applied Mathematics,* March 22-24, 2007, Dallas, Texas.